Applied Catalysis A: General 404 (2011) 30–38

Contents lists available at ScienceDirect

Applied Catalysis A: General

journal homepage: www.elsevier.com/locate/apcata

Inhibition of the hydrogenation of tetralin by nitrogen and sulfur compounds over Ir/SBA-16

Gerardo Simón Balangero Bottazzi, María Laura Martínez, Marcos Bruno Gómez Costa, Oscar Alfredo Anunziata, Andrea Raquel Beltramone *

Grupo Fisicoquímica de Nuevos Materiales, CITeQ, Facultad Córdoba, Universidad Tecnológica Nacional, Maestro López y Cruz Roja Argentina, 5016 Córdoba, Argentina

ARTICLE INFO

Article history:
Received 19 March 2011
Received in revised form 4 July 2011
Accepted 6 July 2011
Available online 18 July 2011

Keywords:
Iridium containing SBA-16
Hydrogenation
Inhibition
Reaction kinetic
Sulfur
Nitrogen compounds

ABSTRACT

In this work we study the catalytic properties of 5 wt.% Ir-containing SBA-16 catalysts (with and without aluminum as heteroatom), in the hydrogenation of tetralin to decalin, in the presence of 100 ppm of N as quinoline, indole and carbazole, and 100 ppm of S as dibenzothiophene and 4,6-dimethyl-dibenzothiophene at 250 °C and 15 atm of pressure of hydrogen, using a Parr reactor. Ir/SBA-16 and Ir/Al-SBA-16 were prepared by wetness impregnation using Iridium Acetylacetonate as source of Ir. The Ir/SBA-16 catalyst synthesized by us had high activity measured in tetralin hydrogenation at mild conditions. The experimental data was quantitatively represented by a modified Langmuir–Hinshelwood type rate equation, using the apparent adsorption constants calculated from the inhibition results for the individual compounds. The catalyst showed a good resistance to sulfur and nitrogen compounds. The inhibiting effect increased in the order: DBT < quinoline < 4,6-dimethyl-DBT < indole < carbazole. The inhibiting effect of the nitrogen/sulfur compounds was strong, but the activity was still higher than with commercial NiMo/alumina catalyst.

We present in this contribution a successfully developed, high loaded and well dispersed Ir/SBA-16 catalysts, that have been shown to maintain a useful catalytic activity, even in the presence of relatively high amounts of sulfur compounds (up to 100 ppm, sulfur basis). Consequently, economically successful processes have evolved, based on this class of catalysts.

1. Introduction

Hydrotreating technology (HDT) is one of the most commonly used refinery processes, designed to remove contaminants such as sulfur, nitrogen, condensed ring aromatics, or metals. The feedstock used in the process range from naphtha to vacuum residue, and the products in most applications are used as environmentally acceptable clean fuels. The process operates at elevated pressure and temperature and consumes hydrogen. Recent regulatory requirements to produce ultra-low-sulfur diesel (ULSD) and gasoline, have created a very dynamic market as refiners must build new or revamp their existing assets to produce the 'green' fuels. To meet this challenge, scientists elsewhere are researching to address the refiner's specific configurations and provide optimized and economically attractive solutions.

The development of highly active and selective hydrotreating catalysts is one of the most pressing problems facing the petroleum industry. Numerous approaches have been adopted with a view to improving the catalytic performance of the classical formulation (Co(Ni)Mo(W)/Al_2O_3) [1–11]. Regarding new support materials, mesoporous molecular sieves such as MCM-41, HMS or SBA-15 [12–15] are promising candidates because of their uniform mesoporous structure, which facilitates the diffusion of the large molecules involved in hydrotreating reactions. Compared with MCM-41 and HMS, the SBA-15 material synthesized under an acidic medium using neutral organic triblock copolymers as structure-directing agents [15,16] seems to be more interesting. Fierro et al. [17] used with success CoMo/Ti-SBA-15 catalysts for dibenzothiophene desulfurization, but the information about SBA-16 support is poor. The SBA-16 silica mesophase with a cubic *Im*3*m* structure was prepared first by Zhao et al. [18] from the triblock copolymer surfactant Pluronic F127 (EO106PO70EO106) and TEOS. The synthesis parameters have been systematically investigated by Mesa et al. [19]. The mesoporosity of this phase consists of two non-interpenetrating three-dimensional channel systems with spherical cavities at the dividing of the channels. It can be expected that this structure offer more interesting opportunities for catalytic applications involving well-dispersed metal-supported catalysts and allowing the diffusion of large molecules.

The purely siliceous SBA's materials have only silanol groups on their surface, which are of low acid strength and catalytically non-active. Therefore, in order to make these materials

* Corresponding author. Tel.: +54 351 4690585; fax: +54 351 4690585.
E-mail address: abeltramone@scdt.frc.utn.edu.ar (A.R. Beltramone).

0926-860X/$ – see front matter © 2011 Elsevier B.V. All rights reserved.
doi:10.1016/j.apcata.2011.07.003

useful for catalysis, stronger acidic sites have to be introduced into their framework. Generally, the substitution of heteroatoms with valence lower than silicon creates negative charges in the framework, which can be compensated by protons, thus generating acidity in these materials. Many investigations have indicated that Al-SBA-15 materials show much higher catalytic activity, compared with Al-MCM-41 [20,21]. The incorporation of Al is particularly important as it gives rise to solid acid materials with acid sites associated with the presence of Al in framework positions, within the silica pore walls. Mesoporous aluminosilicates have therefore, been the focus of many recent studies [22–24], because of their potential application in solid acid/base catalysis for bulky molecules activation. The traditional method of introducing Al into mesoporous silicates is the direct (mixed-gel) synthesis where, an aluminum–silicate framework is formed directly from aluminate and silicate ions.

However, it is very difficult to introduce the metal ions directly into SBA's due to the easy dissociation of metal–O–Si bonds under strong acidic conditions. Thus, the post-synthesis method for the alumination of the mesoporous silica, which are obtained under strongly acid conditions, becomes an appealing alternative [25]. Many studies have shown that aluminum can be effectively incorporated into siliceous MCM-41 and MCM-48 materials via various post-synthesis procedures. The authors claimed that the materials produced via the post-synthesis method have superior structural integrity, acidity, and catalytic activity than those of materials having aluminum incorporated during synthesis [26–29]. Recently Anunziata et al. [30] have published the synthesis of Na-Al-SBA-3 by the treatment of pure silica SBA-3 with an aqueous solution of $NaAlO_2$ at room temperature. In that work, we obtained a material with high-framework aluminum contents, without any significant loss in textural properties of SBA-3.

Some alumina-supported transition metal catalysts possessed much higher hydrodenitrogenation (HDN) and hydrodesulfurization (HDS) activity than a conventional NiMo system [31–35]. For example: Rh, Ir, Ru and Pt supported on silica or alumina are known to catalyze effectively the nitrogen removal from methylamine, quinoline or pyridine also in the reduced state [36]. Noble metal sulfides, either unsupported as bulk compounds [37] or supported on active carbon [38] have been studied extensively in hydrorefining. It has been shown that transition metal sulfides of the 2nd and 3rd rows such as Ru, Rh, Os and Ir were especially active during HDS reactions [37]. Similarly, sulfides of Ir, Os and Re were most active in HDN of quinoline [38] and sulfides of Ir and Pt in HDN of pyridine [39]. However, these catalysts have a low tolerance to sulfur and nitrogen poisoning, therefore a previous deep hydrodesulfurization and hydrodenitrogenation charge pre-treatment is required. This two-stage hydrodearomatization (HDA) process has a high operating cost and, consequently, the development of noble metal-based catalysts with tolerance to sulfur and nitrogen has become attractive. In this case, noble metal-based catalysts are an interesting alternative, since they have high activity for hydrogenation of aromatic hydrocarbons, and the process can then perform at low temperatures and pressures. Recently, much interest has arisen in zeolite-supported noble metal catalysts in connection with their application to the hydrogenation of aromatic hydrocarbons contained in petroleum distillates [40] This is because these catalysts have been shown to maintain a useful catalytic activity, even in the presence of relatively high amounts of sulfur compounds (up to several hundred ppm, sulfur basis) [32,41–43]. Consequently, economically successful processes have evolved, based on this class of catalysts. It is of interest that Ir catalysts display also very high HDN/HDS selectivity. This has already been observed during the study of simultaneous reaction of thiophene and pyridine over a carbon supported Ir catalyst at 280 °C [44] and confirmed more recently for alumina supported Ir catalysts at 320 and 360 °C [45,46]. Similarly, Liaw and co-workers observed that an Ir/Al_2O_3 catalyst showed much higher HDN/HDS selectivity than other noble metal catalysts in hydrotreating of coal-derived naphtha [47].

However, catalytic properties of metal or metal sulfides deposited on alumina or other supports have been studied less frequently and moreover, the major attention up to now has been devoted only to Ru [48]. It was shown by Cinibulk and VõÂ [45] that the HDN activity of an alumina-supported Ir catalyst during the parallel HDN/HDS reaction of pyridine and thiophene was markedly higher than the activity of a Pt catalyst. On the other hand, in comparison to NiMo/alumina the extent of quinoline HDN was only higher for zeolite-supported Ru sulfide (3.5% Ru), the other zeolite-supported noble metal sulfides including Ir (0.8%) were less active [4]. Besides HDN, a high hydrogenolytic activity of Ir has been also well established during studies of hydrocarbon reactions in connection with naphtha reforming [36,49,50]. Factors such as the effect of catalyst preparation and metal dispersion have often been studied in connection with this process [36,50–53]. The results obtained in all these studies suggest that Ir could be an efficient active phase for the transformation of aromatics to saturated compounds and efficient for sulfur and nitrogen removal, by either itself or as a promoter of conventional catalysts. However, the data about the effects of Ir dispersion in different supports in hydrogenation (HYD) and HDS/HDN reactions are not available in the literature at present.

Nitrogen and sulfur compounds naturally occurring in atmospheric gas oil (AGO) and light cycle oil (LCO), used as feedstocks for diesel fuel production, are traditionally considered as being responsible for color and gum formation. Moreover, they have been identified as strong inhibitors of the hydrogenation (HYD) reactions during the hydrotreatment process [54,55], even when they are present in very low concentrations [56,57]. Usually, the basic nitrogen compounds have been considered stronger inhibitors for the HYD and HDS reactions than the non-basic moieties [54,55]. However, strong inhibition of these reactions by non-basic nitrogen compounds has been observed, either due to hydrogenation (HYD) reactions occurring during this process, that lead to the formation of basic species [58,59], or to a strong adsorption of the non-basic compounds over the support surface [60–62]. For carbazole, Nagai and Kabe [58] and LaVopa and Satterfield [63] reported a strong inhibiting effect on the thiophene and dibenzothiophene HDS reactions, comparable to those of the basic compounds pyridine, piperidine and acridine. The high value of the adsorption characterizing carbazole was attributed to products of a rapid hydrogenation converting it to basic compounds. Nitrogen- and sulfur containing compounds inhibit HYD through competitive adsorption. Although interesting information about the inhibition effect from nitrogen compounds has been forwarded by previous studies [60–62], moreover, the majority of the studies have focused on the nitrogen inhibition effect on the HDS reaction and therefore systematic information related to the inhibition effect on HYD reactions is scarce.

LaVopa and Satterfield [63] developed a Langmuir–Hinshelwood (L–H) type equation to describe the poisoning effect of nitrogen compounds during DBT HDS. Recently, the inhibition effect on HYD reactions, was experimentally determined by Beltramone et al. [9,10] using a commercial $NiMo/Al_2O_3$ catalyst at pressures and temperatures commonly used in the hydrotreatment of diesel and at sulfur and nitrogen concentrations relevant to deep HDS.

Tetralin is one of the most representative and refractory molecules of aromatics presents in diesel pool, for that reason we choose tetralin as a model molecule to study the activity of the catalyst and the inhibition effect. The information available in the literature about inhibition effects observed during the hydrogenation of tetralin in the presence of sulfur and nitrogen compounds over Ir containing mesoporous catalysts is scarce and contradictory

and the inhibiting effect of N and S over tetralin hydrogenation using Ir/SBA-16 is not reported elsewhere. Consequently, the main objective of this work is to present L–H type equations that quantitatively describe the inhibition effect observed during HYD of tetralin in the presence of dibenzothiophene (DBT) and 4,6-dimethyl-dibenzothiophene (4,6-DMDBT), carbazole, indole and quinoline, using a batch reactor at softer conditions than used in industrial processes.

2. Experimental

2.1. Synthesis of Si-SBA-16 and Al-SBA-16

Mesoporous silica materials with cubic *Im*3*m* structure were synthesized according to the procedure described by Kim et al. [64]. Briefly, poly (alkylene oxide)-type triblock copolymers; F127 (EO106PO70EO106, MW 5 12600) were dissolved in aqueous HCl solution. Tetraethyl orthosilicate was added to the solution at 35 °C under continuous stirring during 15 min at that temperature. The molar composition of the mixture was as follows: F127/TEOS/HCl/H_2O = 0.004/1/4/130. This mixture was kept under static conditions in an oven for 6 h at the same temperature. Subsequently, the mixture was placed in an oven at 50 °C, over a period of 20 h; afterwards the temperature of furnace was increased to 80 °C for aging for 20 h, after that, the solid product was recovered by filtration and dried at 100 °C. The Si-SBA-16 sample was immersed in ethanol reflux for 6 h, to extract the surfactant and then was calcined at 550 °C in air for 6 h. The material obtained was identified as SBA-16. The alumination procedure of SBA-16 was carried out as follows: Silica SBA-16 (1 g) was stirred in 50 ml of water, containing dissolved sodium-aluminate, at room temperature for 20 h and pH of 5.6. The synthesis was performed at this pH, because sodium aluminate is not stable in acid medium (pH < 3), and it reacts rapidly with protons to generate aqueous Al^{3+} ions. When pH is enough high, deposition of aluminum hydroxide will occur. The mixture was filtered, washed, dried at room temperature overnight and then calcined in air at 550 °C for 5 h. Finally, Al-SBA-16 sample with theoretical Si/Al = 20 was obtained.

2.1.1. Synthesis of Ir/SBA-16 and Ir/Al-SBA-16

The samples were prepared using Iridium Acetylacetonate (Aldrich 99.9% Ir(Acac)3) as source of Ir. Iridium was incorporated by wetness impregnation employing ethanol as solvent, due to its very low solubility in water. The obtained powder was then dried at 80 °C overnight, and then calcined at 500 °C for 5 h. After that, the samples were desorbed in inert atmosphere from 25 °C to 200 °C with a slope of 10 °C/min and kept at this temperature during 5 h, after that the temperature was increased to 470 °C with a slope of 10 °C/min, kept 5 h at that temperature. Nitrogen flow was always 20 ml/min. Due to iridium is active for the reaction in its metallic state; it was reduced in H_2 flow of 20 ml/min, at 470 °C using the same procedure described above. The iridium load was 5 wt.% and the samples obtained were denoted as Ir/SBA-16 and Ir/Al-SBA-16.

2.2. Characterization of the catalysts

Infrared measurements were performed with a JASCO 5300 FTIR spectrometer. For structure (fingerprint zone) characterization, samples of SBA were mixed with KBr (0.05 wt.% catalyst/99.95 wt.% KBr), and pressed forming a wafer.

The XRD patterns were collected by using a continuous scan mode with a scan speed of 0.02° (2θ)/min. XRD patterns were recorded in the Philips X'Pert PRO PANalytical diffractometer, operating with CuKa X-ray radiation (X-ray generator current and voltage set at 40 mA and 45 kV), using small divergence and scattering slits of 1/32 mm and a goniometer speed of 1.2° (2θ)/min. The scanning range was set between 0.5° and 5°. The sample was crushed previously and placed it in an aluminum sample holder.

Scanning electron micrographs (SEM) were obtained by using a nova NANOSEM 230 Phillips with EDAX. Samples were placed over an aluminum drum and covered with a gold film, using a JEOL Ion Sputter JFC 1100.

TEM observations were performed in a Philips CM 200 UT transmission electron microscope at Centro Atómico Bariloche. Samples for TEM were prepared by dispersing a small amount of powder in ethanol and depositing a drop of the resulting suspension on a commercial carbon coated copper grid.

Elemental analysis was performed by inductively coupled plasma-atomic emission spectroscopy (VISTA-MPX) operated with high frequency emission power of 1.5 kW and plasma airflow of 12.0 L/min. The surface area was determined by the BET method using a MICROMERITICS Chemisorb 2720 apparatus, equipped with a TCD detector.

Hydrogen chemisorption characterization was performed in a Chemisorb 2720 Micromeritics, measured at temperature pulses and at atmospheric pressure. The samples were previously treated and reduced. For the hydrogen chemisorption, we assumed a stoichiometric value of 2 H/Ir. The accuracy/reproducibility to the results is typically better than ±1.5% with ±0.5% reproducibility. The metal dispersion value is determined by Eq. (1):

$$\%D = S_f \times \frac{V_{ads}}{V_g} \times \frac{\text{m.w.}}{\%M} \times 100\% \times 100\% \quad (1)$$

where S_f = stoichiometry factor (2), considering the dissociation of H_2 adsorbed onto Ir atom, V_{ads} = volume adsorbed (cm^3/g) V_g = molar volume of gas at SPT (22.414 cm^3/mol), m.w. = molecular weight of the metal (192.217 a.m.u.), $\%M$ = % metal (4.9–5.1% of Ir in our case), $\%D$ = percent of metal dispersion (%).

The active metal surface area per gram of sample, (m^2/g sample) was calculated by the following equation:

$$\text{MSA}_s = S_f \times \frac{V_{ads}}{V_g} \times \text{NA} \times \sigma_m \times \frac{m^2}{10^{18}\ \text{nm}^2} \quad (2)$$

where S_f = stoichiometry factor (2), V_{ads} = volume adsorbed (cm^3/g), V_g = molar volume of gas at SPT (22.414 cm^3/mol), NA = Avogadro's number (6.023×10^{23} molecules/mol), σ_m = cross-sectional area of active metal (0.074 nm^2), MSA_s = active metal surface area per gram of sample.

2.3. Catalytic activity

The catalytic activity was measured in a Parr reactor 4563, at 250 °C, 15 atm of pressure of hydrogen and 360 rpm.The feed consisted in 50 ml of 5% v/v of tetralin (98.5% FLUKA) in dodecane in presence of 100 ppm of S or N in the respective cases. The products were analyzed with a HP 5890 Series II GC and HP-5 column. The activity of the catalysts was compared with an Ir/Al_2O_3 sample prepared with Commercial γ-Al_2O_3 (Topsoe, M-80T) and Ir incorporated with the same procedure described for SBA-16; the results were also compared with a typical HDT catalyst as $NiMo/Al_2O_3$ Criterion 424.

3. Results and discussion

3.1. Characterization of the catalysts

3.1.1. IR spectroscopic studies

Fig. 1 shows the spectrum of Si-SBA-16 and Al-SBA-16 in the same fingerprint region. We can observe that a signal at around 970 cm^{-1}, which is assigned to asymmetric stretching of Si–O bond neighboring surface silanol groups, was emerged on the spectra of the pristine SBA-16 sample. However, this band is absent

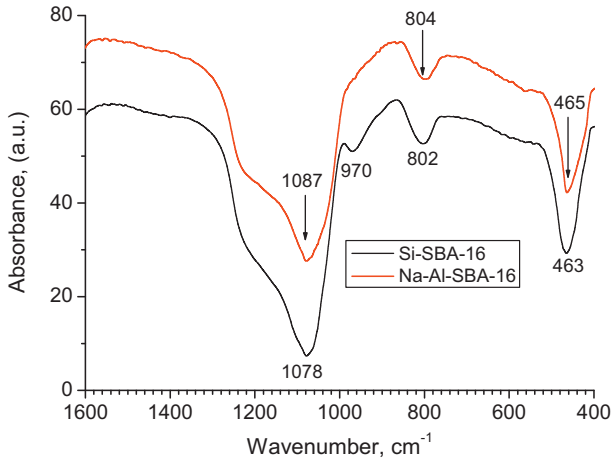

Fig. 1. FTIR of SBA-16 and Al-SBA-16.

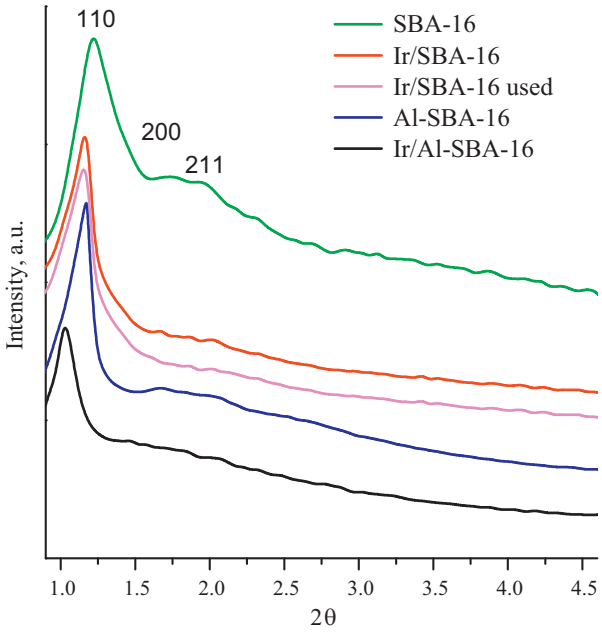

Fig. 2. XRD pattern of SBA-16 synthesized samples.

when SBA-16 was post-aluminated, which indicated that the surface silanol groups around 969–970 cm^{-1} interacted with the Al species and contributed to form the Si–O–Al bonds, in the process of modification. The presence of asymmetric stretching T–O (T = Si, Al) can be observed in the samples at 1232 and 1078 cm^{-1}, due to external tetrahedral TO4 vibrations of weak intensity and internal tetrahedral TO4 vibrations of strong intensity, respectively. Siliceous SBA-16 samples show a band at 800–802 cm^{-1}, due to Si–O–Si symmetric stretching modes and another stronger band at 461–465 cm^{-1}, due to rocking Si–O–Si, respectively [30]. The spectra of the Al-SBA-16 material show additional features in the vicinity of the 1087 and 804 cm^{-1} stretching bands, which absorption frequency shifts upward, with aluminum incorporation into the pristine sample. These features can be assigned to Al–O–Si bending vibrations, indicating incorporation of aluminum into the SBA-16 silica matrix [30]. Thus, the substitution of silicon by aluminum causes shifts of the lattice vibration bands to higher wavenumbers.

3.1.2. XRD studies

For determination of the structure and symmetry of the materials, XRD patterns were analyzed. SBA-16 with cubic *Im*3*m* structure is a body-centered-cubic arrangement of cages with 8 apertures to the nearest neighbors. The unit-cell parameter, a_0 (Table 1), of the crystallographic structure was obtained by solving the following equation depending on the type of space group: $a_0 = d_{hkl} \cdot \sqrt{(Q_{hkl})}$, where Q_{hkl} is: $Q_{hkl} = h^2 + k^2 + l^2$, for a cubic space group like the cubic body centered (*Im*3*m*) SBA-16. A typical X-ray diffractogram of SBA-16 is expected to present peaks at $2\theta < 3^\circ$, corresponding to an *Im*3*m* cubic structure [16,65], however, many often just the first two peaks have been clearly detected [66–68]. The X-ray diffractograms of the SBA-16, Ir-SBA-16 and the mesostructured Al-SBA-16 and Ir-AlSBA-16 are shown in Fig. 2. The XRD pattern of calcined SBA-16 sample shows a very strong (1 1 0) reflection (1.2° 2θ) of the cubic *Im*3*m* structure and two small shoulders of the (2 0 0) and (2 1 1) reflections (1.7° and 1.92° 2θ, respectively). All these reflections yield an a_0 value of 12.16 nm, confirming that the measured structure is indeed the *Im*3*m* structure [69,70]. Similar XRD pattern was also observed for the Al-SBA-16 sample (Fig. 2). However, in this case the positions of (1 1 0), (2 0 0) and (2 1 1) reflections were shifted to 1.11, 1.68 and 1.81° 2θ, respectively, giving a_0 a value of 13.1 nm. In the case of the aluminum containing material, only the peak indexed as [1 1 0] is clearly observed, probably because the aluminum insertion leads to a structure with lower order [24]. It has to be mentioned for the sake of clarity that some publications report on the preparation of materials with disordered pore organization with X-ray patterns displaying a single peak, which was related to the SBA-16 structure [14]. Although it is known that aluminum containing MCM-41 is less ordered than the pure silica parent material [71], and that it is highly probable that this behavior is similar for the AlSBA-16. The signals at the corresponding Miller indices indicate that the ordered mesoporous structure is preserved during aluminosilicates synthesis.

In line with this, a characteristic (1 1 0) reflection of *Im*3*m* structure is still observed in the XRD pattern of Ir/SBA-16 (Fig. 2). XRD results suggest that the mesoporous cage-like structure of SBA-16 was maintained during the course of the preparation of Ir modified catalysts. However, a significant decrease in its intensity and broadening after Ir deposition suggest some loss in the periodicity of the SBA-16 pore structure. Therefore, a strong obstruction of the support pores after metal deposition could be supposed to occur in this catalyst.

Table 1
Structural characteristics of SBA-16 samples.

Samples	2θ			d (Å)			a_0 (nm)[a,b]
hkl	1 1 0	2 0 0	2 1 1	1 1 0	2 0 0	2 1 1	
SBA-16	1.20	1.70	1.92	85.67	60.82	49.65	12.16
Ir/SBA-16	1.17	1.75	1.92	86.70	61.40	50.50	12.30
Al-SBA-16	1.11	1.68	1.81	92.60	65.85	50.70	13.10
Ir/Al-SBA-16	1.02	1.61	1.72	86.00	61.80	43.60	14.16

[a] $a_0 = d200\sqrt{4}$.
[b] $D \cong 4\,V/A$; (according to Refs. [72,73]).

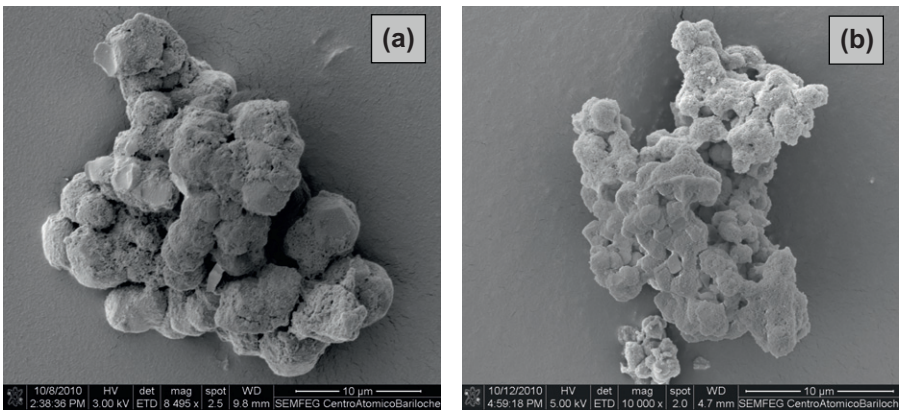

Fig. 3. SEM micrographs of Ir/SBA-16 (a) and Ir/Al-SBA-16 (b).

We also can observe in Fig. 2, a pattern for Ir/SBA-16 used, this pattern shows that the structure remains unalterable, even after three cycles of reaction.

3.1.3. SEM and TEM characterization

The size and shape of the samples indicate good morphology of the crystals, without other phases, typical of these materials (Fig. 3a and b). As shown in Fig. 3a for Ir/SBA-16 sample, the particles have a spherulictic shape; the particle size of the Ir/SBA-16 is 4–5.0 μm in diameter, whereas the crystal of Ir/Al-SBA-16 is almost spherulictic with a lower particle size (2–3 μm).

The TEM image of the SBA-16 mesoporous silica crystal, exhibits the well-ordered *Im*3*m* cubic mesostructures (Fig. 4b), confirmed by XRD data of SBA-16 single crystals having a well-ordered mesostructure. According to Fig. 4a and b, the Ir clusters size is bigger in Ir/Al-SBA-16 than in Ir/SBA-16 samples, in agreement with the data shown in Table 2, obtained by H_2 chemisorption.

The physicochemical properties of the samples (supports and catalysts) are summarized in Table 2. The results of ICP elemental analysis, which was employed to determine the composition of Al-SBA-16 sample, indicated the amounts of the heteroatom (Al) in the final Al-SBA-16 support, are in close agreement with theoretical value, Si/Al = 19.8. The BET specific surface area decreases with the Al content, from 870 (SBA-16) to 700 m^2/g for Al-SBA-16, due to the occupation of guest species on the surface of the pores, as well as the in equable contribution of the additional mass Al_2O_3 in the sample. The iridium content in the samples was determined by ICP. The dispersion and mean clusters sizes in the reduced catalysts by H_2 pulse adsorption at 22 °C. The catalyst (0.5 g) was in situ reduced by H_2 (30 ml/min) at 400 °C for 2 h and purged by N_2 (25 ml/min) at 400 °C for an additional 0.5 h. The samples were cooled to 22 °C, and titrated by H_2 pulses in a stream of N_2, until constant output TCD signal indicated saturation. The mean diameter of the Ir particles was estimated under the basic assumption of stoichiometry for H/Ir = 2, with spherical shape of the metal particles. As it was mentioned in TEM studies, lower particle size and higher dispersion of metallic Ir was found in SBA-16 without Al in its structure than in Ir/Al-SBA-16 (*D* = 40 and 35% respectively, see Table 2), with relative similar Ir content.

3.2. Catalytic activity

Unlike olefins hydrogenation, high hydrogen pressures are required to outcome ring saturation in aromatics hydrogenation. This is in part due to the low reactivity of the aromatic structure as a result of resonance stabilization of the conjugated system and, partly due to limitations determined by the thermodynamic equilibrium at the pressures and temperatures employed. Therefore, most studies on the reactivity of aromatics have been conducted at pressures and temperatures that favor low equilibrium concentrations of aromatics. Despite of the industrial conditions that use high pressure and temperature, we are addressing here, more active catalyst in order to perform at mild conditions and in a batch reactor.

In order to find the best operation conditions, the hydrogenation reaction was previously tested at different conditions: at atmospheric pressure the catalyst exhibited dramatic decrease of the tetralin conversion values by increasing the reaction temperature, due to the thermodynamic constraints of the reaction. At 300 °C the fully hydrogenated products were not more detected, while, together with tetralin, traces of high-molecular-weight, ring-opening products and low-molecular-weight, cracking products were formed. While at atmospheric pressure Ir/SBA-16 showed a low hydrogenation activity, in the tests performed at higher pressures than 15 atm the catalytic activity slightly grew, compared

Table 2
Physicochemical properties of the supports and catalysts.

	SBA-16	Ir/SBA-16	Al-SBA-16	Ir/Al-SBA-16	Ir/Al_2O_3
Si/Al[a]	–	–	19.8	19.8	
Area, m^2/g	870	550	700	480	150
Ir, wt.%[a]	–	4.9	–	5.1	4.8
Mean crystal size, μm[b]	4.8	4.5	3.0	2.5	3.5
Metal dispersion, %		40.0		35.0	26.0
Metal surface area, m^2/g sample		4.54		4.14	2.89
Metal surface area, m^2/g metal		92.75		81.16	60.29
Particle diameter, nm		2.9[c]		3.3[c]	4.4[c]
		3[d]		3.5[d]	4.8[d]

[a] Data obtained by ICP.
[b] SEM.
[c] From metal dispersion obtained by hydrogen chemisorption.
[d] From TEM.

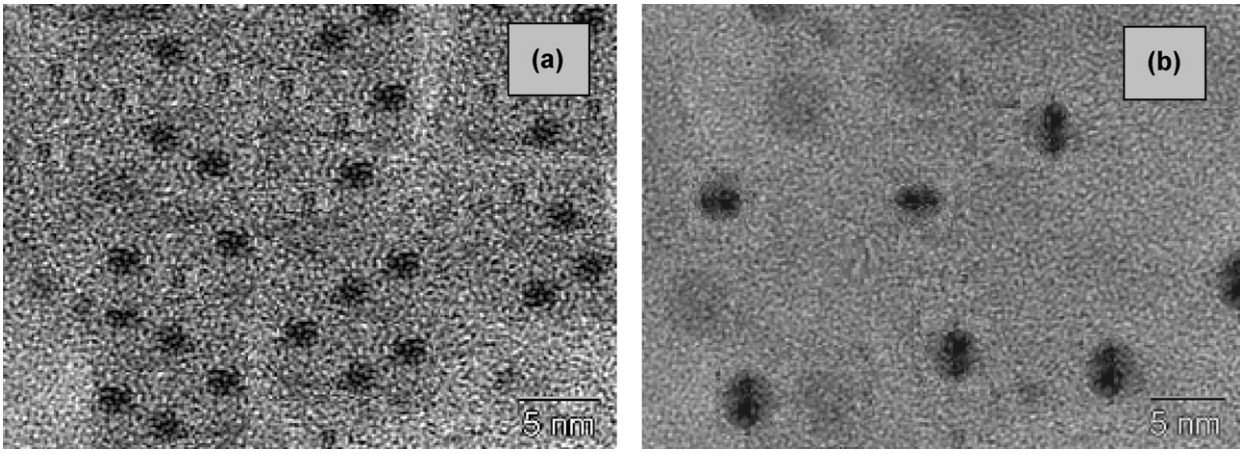

Fig. 4. TEM images of Ir/SBA-16 (a) and Ir/Al-SBA-16 (b).

with the test at 15 atm. However, all the catalysts required a large H2 excess, to avoid a decrease in hydrogenation and ring-opening activity, and gave rise to the best performance for the studied contact time, favoring at lower values the total hydrogenation to decalin and no cracking reactions at 250 °C. On the other hand, at high pressures, the increase of temperature favored the formation of the ring-opening and, mainly, cracking products. Furthermore, this may supply useful information on the behavior of Ir-catalysts, claimed as active and stable in dearomatization and ring-opening reactions.

The results are shown in Table 3, the catalytic activity of the synthesized samples and a commercial $NiMo/Al_2O_3$ catalyst was compared.

The hydrogenation reactions of tetralin were carried out at 250 °C and 15 atm in the presence of traces of DBT. The major products were trans-decalin, cis-decalin, and naphthalene. Trans-decalin was the product with the highest initial selectivity, followed by cis-decalin and naphthalene. The trans isomer is expected to be favored based on thermodynamic calculations. In addition to the hydrogenation, dehydrogenation of tetralin to naphthalene took place during the hydrogenation of tetralin, even though the experiments were performed far below the thermodynamic equilibrium. The naphthalene formation was dependent on the tetralin concentration and the hydrogenation rate. A high tetralin concentration together with a low hydrogenation rate favored the naphthalene formation. The dehydrogenation was nevertheless a minor reaction and only traces of naphthalene were formed. Sapre and Gates [74] and Korre et al. [75] have reported a similar reversible dehydrogenation–hydrogenation reaction for tetralin and naphthalene on a sulfided CoMo-catalyst. Decalins appeared to be fairly unreactive under these conditions, while naphthalene hydrogenated back into tetralin.

According to the data shown in Table 3, the selective conversion of tetralin to decalin using Ir/SBA-16 is higher than Ir/Al-SBA-16, Ir/Al_2O_3 and 60% higher than $NiMo/Al_2O_3$, respectively. Is interesting to analyze the activity comparing the turn over number (TON) (see Table 3). The turn over number was calculated considering the σ_m = cross-sectional area of active metal (0.074 nm^2) and the active metal surface area per gram of sample, according H_2 chemisorption. Thus, TON is very similar, suggesting that the higher conversion levels are due to the higher Ir atoms dispersion as active center to the reaction. Differences in activity, as it was mentioned could be due to the better iridium dispersion obtained on SBA-16 used as support (see Tables 2 and 3). Ir/SBA-16 also showed a high activity even in presence of sulfur compared with a typical NiMo catalyst.

Table 3
Catalytic activity results. Feed: 0.05 mol of tetralin/g of catalyst in dodecane, 100 ppm of sulfur as DBT were added. T = 250 °C, P = 15 atm. Reaction time 8 h, stirring = 60 rpm.

Samples	Conv. of tetralin (mol%)	TON × 10^6
Ir/SBA-16	80	0.13[a]
Ir/Al-SBA-16	68	0.12[a]
Ir/Al_2O_3	63	0.11[a]
$NiMo/Al_2O_3$ Criterion 424	20	

[a] Calculated using the Ir metal surface area, m^2/g sample and cross-sectional area of active metal (0.074 nm^2).

According previous studies performed by Klimova et al. [14], NiMo catalysts supported on Al-containing SBA-16 molecular sieves, which were prepared by grafting with $AlCl_3$ or $Al(i\text{-}PrO)_3$, show high activity in HDS of refractory dibenzothiophenes (4,6-DMDBT). This can be attributed to good dispersion of Ni and Mo active phases and to the bifunctional character of these catalysts, namely, to the participation of both types of sites: active sites of NiMoS phase and Bronsted acid sites of the support in the catalytic transformations of 4,6-DMDBT. Therefore, high catalytic performance of these catalysts in HDS of refractory DBTs can be attributed to the synergism between both types of active sites. The interaction of Ni and Mo species with the support becomes stronger with Al loading into the SBA-16 by post-synthetic aluminum grafting. According to this, the dispersion of sulfided Mo species increases. However, when SBA-16 is aluminated using $NaAlO_2$, NiMo catalysts with low surface area and activity are obtained. This point out the method of incorporation of Aluminum into the SBA-type materials and Al sources suitable for the preparation of supports for HDS catalysts.

In our case is possible to see, that post-synthesis alumination of SBA-16, by reacting with $NaAlO_2$ leads to an important decrease of surface area comparing with the parent material. We obtained also, a catalyst with lower dispersion than the parent SBA-16 without aluminum. This activity trend with the change of the Al-containing SBA-16-support would be the result of too strong metal–support interaction, as in the case on Ir/Al-SBA-16 catalyst that makes the reduction of Ir species more difficult. This could be joint with Ir dispersion, other reason of the lower activity of Ir/Al-SBA-16 compared with Ir/SBA-16.

In order to study the behavior of Ir/SBA-16 in presence of N and S compound, computation of kinetic parameters was required to shed further light on this issue; the data can be used to provide a better value for the constraints used to obtain the rate constants in the model.

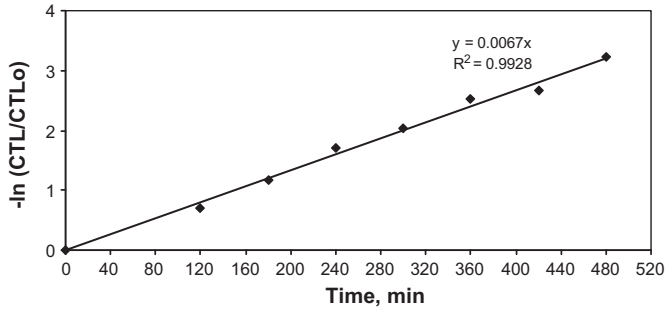

Fig. 5. First-order behavior of the tetralin hydrogenation without inhibitors at 250 °C and 15 atm, over Ir-SBA-16.

Generalized Langmuir–Hinshelwood rate equation can be used to represent the inhibiting effect of nitrogen containing compounds as quinoline, indole, carbazole and sulfur containing compounds as dibenzothiophene and 4,6-dimethyl-dibenzothiophene on the tetralin hydrogenation.

3.3. Kinetic calculations

First-order tetralin hydrogenation rate constants, based on the rate of tetralin disappearance were calculated using the integral method. The tetralin conversion showed a first-order behavior when graphing $\ln(CTL/CTL_o)$ versus time (Fig. 5). The slope and the correlation coefficient were calculated via least-squares fitting. Correlation coefficients higher than 0.96 were obtained in all cases. Trans-decalin and cis-decalin were observed as the main products of the tetralin hydrogenation reaction (more than 98%). The semiempirical kinetic model proposed is the generalized Langmuir–Hinshelwood model for hydrogenation, for tetralin hydrogenation, the reaction rate is given by:

$$r_{TL} = \frac{kK_{TL}C_{TL}}{1 + K_{TL}C_{TL}} \times \frac{K_{H_2}C_{H_2}}{1 + K_{H_2}C_{H_2}} \quad (3)$$

where r_{TL} is the tetralin conversion to decalins rate, C_{TL} is tetralin concentration and C_{H_2} is hydrogen concentration, k is the rate constant and K is the adsorption equilibrium constants of the individual compounds. Under our experimental conditions, $K_{H_2}C_{H_2} \gg 1$, therefore, this kinetic equation could be simplified:

$$r_{TL} = \frac{kK_{TL}C_{TL}}{1 + K_{TL}C_{TL}} \quad (4)$$

The kinetic calculations showed a first-order behavior with respect to the tetralin concentration, and the value of the $K_{TL}C_{TL}$ product was close to 0. Substituting the kK_{TL} product by k_{TL}, Eq. (4) was further simplified to:

$$r_{TL} = k_{TL}C_{TL} \quad (5)$$

The value obtained for k_{TL} at 250 °C (Fig. 5) using the integral method, already described, was 6.7×10^{-2}/min ($R^2 = 0.99$). This value will be used as a reference for the results obtained in the experiments where this reaction was inhibited by nitrogen or sulfur compounds.

3.3.1. Control of the kinetic regime

A set of experiments was performed to check the absence of intraparticle and interphase mass transfer limitations. Different sizes of catalyst particles (0.2, 0.4, 0.6, 0.8 mm) were tested and the results indicated that a kinetic regime was established in all cases.

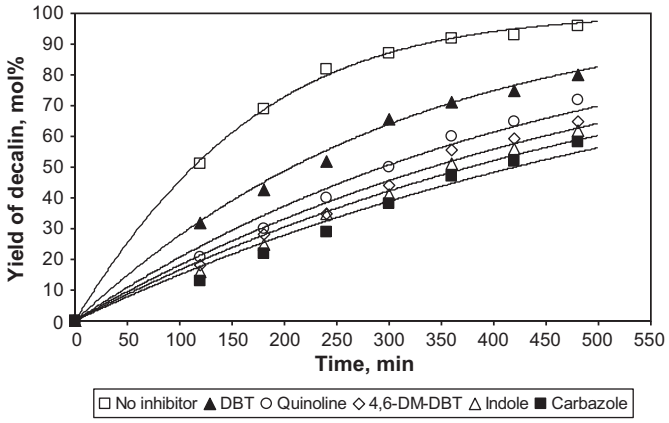

Fig. 6. Kinetic of the hydrogenation of tetralin at $T = 250$ °C, $P = 15$ atm, 360 rpm. The lines were obtained by fitting the kinetic curves derived from the model to the experimental data ($F = 1, 2^{-3}$).

3.3.2. Kinetic model for tetralin inhibition by sulfur and nitrogen compounds

The hydrogenation of tetralin reaction was carried out at 250 °C and 15 atm in the presence of different nitrogen or sulfur compounds as dibenzothiophene, 4,6-dimethyl-dibenzothiophene, quinoline, indole and carbazole (concentration equivalent to 100 ppm as nitrogen or sulfur). The inhibiting effect in the tetralin hydrogenation was studied according to LaVopa and Satterfield [63], and the following equation was proposed:

$$r_{TL} = \frac{k_{TL}C_{TL}}{1 + K_iC_i} \quad (6)$$

where r_{TL} is the pseudo-first-order rate constant for the reaction inhibited by nitrogen/sulfur compounds, where K_i is the apparent nitrogen/sulfur compound adsorption equilibrium constant (l/mmol) and represents the behavior of all the nitrogen/sulfur compounds that contribute to the inhibition and C_i the initial nitrogen compound concentration (mmol/l). The results of these experiments (Fig. 6) were fitted to a pseudo-first-order rate equation, with correlation coefficients (R^2) better than 0.98 in all cases. The excellent representation of the experimental results by a pseudo-first-order rate equation implies that the inhibition effect is approximately constant during each test. The inhibiting strength does not seem to be affected by the conversion of the parent nitrogen/sulfur compound, the formation or disappearance of basic compounds or the degree of organic nitrogen removal in the case of nitrogen compounds. This behavior suggests that the coverage of the available active sites by nitrogen compounds is established in the early stages of the reaction and remains nearly constant throughout the experiment, probably due to the slow kinetics of desorption of these compounds [55,76]. Therefore, the variation in the nitrogen or sulfur compound concentration along time was not considered in the development of the model. The parameter estimation of the kinetic model was performed with the Powell version of the Levenberg–Marquardt algorithm. The differential equation was solved using the EPISODE package of Scientist®. The objective function (Eq. (7)) was the sum of the squares of the differences between experimental and calculated yields of decalin versus time of the reaction, for each inhibitor in particular (Fig. 6).

$$F = \sum_{1}^{n} (y_{exp} - y_{cal})^2 \quad (7)$$

The inhibiting effect of the compounds included in this study increases in the order: DBT < quinoline < 4,6-dimethyl-DBT < indole < carbazole. The inhibiting effect of these compounds

Table 4
Adsorption constants for the different nitrogen/sulfur compounds derived from the kinetics analysis.

Compound	Adsorption constant K (L/mmol)
Dibenzothiophene	147
Quinoline	280
4,6-Dimethyl-DBT	352
Indole	408
Carbazole	475

is strong at concentrations as high as 100 ppm as nitrogen or sulfur, but still the catalyst is more active than with commercial NiMo/alumina catalyst (i.e. TL mol% conv. obtained at the same conditions in presence of 100 ppm of sulfur as DBT was 60% less at 8 h of reaction). Although, the differences between them are small, the slightly higher inhibiting effect of carbazole and indole, suggests that the inhibiting effect could not be attributed only to hydrogenation reactions converting it into basic compounds [77,78], as it has been suggested by Ho [79] and Odebunmi and Ollis [80]; because if that was the case, all these nitrogen compounds should have the same strength at the same nitrogen concentration. Then, the inhibition behavior seems related to the strong adsorption of the specific nitrogen/sulfur compound directly on the catalyst surface [81–83]. In order to elucidate that fact, the adsorption constants were determined (Table 4). The stronger adsorption would yield a larger adsorption constant, and thus a higher surface coverage. This might be the reason (or partly) for the excellent correlation and the strong inhibiting effect on the hydrogenation and hydrodesulfurization reactions.

4. Conclusions

The Ir-SBA-16 catalyst synthesized by us had high activity measured in tetralin hydrogenation at mild conditions. The good activity was correlated with higher Ir dispersion on SBA-16 mesostructured material used as support, with higher active metal sites exposed to reactant. The kinetic model was successfully applied to the hydrogenation of tetralin in presence of inhibitors. The hydrogenation rates were affected by the competing reactions. The hydrogenation rates of tetralin were low when the inhibitors were present in the mixture. This was explained in terms of competitive adsorption and subsequent inhibition. The inhibition was described reasonably well by Langmuir–Hinshelwood formal kinetic model. Adsorption strength of the inhibitors increased in the order DBT < quinoline < 4,6-dimethy-DBT < indole < carbazole. Adsorption equilibrium constants for the studied nitrogen/sulfur species correlated with the electronic structures. The high inhibiting effect of carbazole and indole could be attributed to hydrogenation reactions converting them into basic compounds or to their polymerization on the catalyst surface. Further experimentation for the development of a complete inhibition mechanism is required. Ir/SBA-16 showed high activity and a good resistance to sulfur and nitrogen compounds. In conclusion, the behavior of iridium inside a mesoporous SBA-16 framework was investigated in the hydrogenation of tetralin, as preliminary step to investigate selective ring opening. The catalyst systems investigated can be used in two-stage operation (moderate H_2 pressure) as S-tolerant noble-metal. It is known that iridium catalyst are more expensive than NiMo catalyst, but it allow to work at lower temperatures and pressures due its higher activity, therefore, the cost of the catalyst are compensated with the saving in the operating conditions and the much higher activity, almost six time higher.

Acknowledgments

Thank to CONICET Argentina, PIP N° 112-200801-00388 (2009–2011); and MINCyT Cba. 1210/07 (2007–2011). Special thanks to Dr. A. Caneiro and Dr. H. Troiani for SEM, TEM analysis.

References

[1] V. Gembicki, T. Cowan, G. Brierley, Hydrocarb. Process 86 (2007) 41.
[2] T. Choudhary, S. Parrott, B. Jonson, Environ. Sci. Technol. 42 (2008) 1944.
[3] C.S. Song, Catal. Today 86 (2003) 211.
[4] T. Choudhary, J. Malandra, J. Green, S. Parrott, B. Johnson, Angew. Chem., Int. Ed. 45 (2006) 3299.
[5] S. Brunet, D. Mey, G. Perot, C. Bouchy, F. Dile, Appl. Catal. A: Gen. 278 (2005) 143.
[6] T. Choudhary, Ind. Eng. Chem. Res. 46 (2007) 8363.
[7] A. Owusu-Boakye, A. Dalai, D. Ferdous, J. Adjaye, Energy Fuels 19 (2005) 1763.
[8] M. Jacquin, D. Jones, J. Roziere, A. Lopez, E. R-Castellon, J. Menado, M. Lenarda, L. Storaro, A. Vaccari, S. Albertazzi, J. Catal. 228 (2004) 447.
[9] A. Beltramone, D. Resasco, W. Alvarez, T. Choudhary, Ind. Eng. Chem. Res. 47 (2008) 7161–7166.
[10] A. Beltramone, S. Crossley, D. Resasco, W. Alvarez, T. Choudhary, Catal. Lett. 123 (2008) 181–185.
[11] E. Furimsky, Appl. Catal. A: Gen. 171 (1998) 177.
[12] G.M. Dhar, G.M. Kumaran, M.j. Kumar, K.S. Rawat, L.D. Sharma, B. David Raju, K.S. Rama Rao, Catal. Today 99 (3/4) (2005) 309.
[13] L. Vradman, M.V. Landau, M. Herskowitz, V. Ezersky, M. Talianker, S. Nikitenko, Y. Koltypin, A. Gedanken, J. Catal. 213 (2003) 163.
[14] T. Klimova, L. Lizama, J.C. Amezcua, P. Roquero, Torres nF E., J. Navarrete, J.M. Dominguez, Catal. Today 98 (2004) 141.
[15] J.C. Amezcua, L. Lizama, C. Salcedo, I. Puente, J.M. Dominguez, T. Klimova, Catal. Today 107/108 (2005) 578.
[16] D. Zhao, J. Feng, Q. Huo, N. Melosh, G. Fredrickson, B.F. Chmelka, G.D. Stucky, Science 279 (1998) 548.
[17] R. Nava, R.A. Ortega, G. Alonso, C. Ornelas, B. Pawelec, J.L.G. Fierro, Catal. Today 127 (2007) 70–84.
[18] D. Zhao, Q. Huo, J. Feng, B.F. Chmelka, J. Am. Chem. Soc. 120 (1998) 6024–6036.
[19] M. Mesa, L. Sierra, J. Patarin, J.-L. Guth, Solid State Sci. 7 (2005) 990–997.
[20] A. Vinu, B.M. Devassy, S.B. Halligudi, W. Bohlmann, M. Hartmann, Appl. Catal. A: Gen. 281 (2005) 207–213.
[21] A. Vinu, D.P. Sawant, K. Ariga, M. Hartmann, S.B. Halligudi, Micropor. Mesopor. Mater. 80 (2005) 195–203.
[22] G.A. Eimer, M.B. Gómez Costa, L.B. Pierella, O.A. Anunziata, J. Colloid Interf. Sci. 263 (2003) 400–407.
[23] W. Hu, Q. Luo, Y. Su, L. Chen, Y. Yue, C. Ye, F. Deng, Micropor. Mesopor. Mater. 92 (2006) 22–30.
[24] J.M.R. Gallo, C. Bisio, L. Marchese, H.O. Pastore, Micropor. Mesopor. Mater. 111 (2008) 632–635.
[25] H.M. Kao, C.C. Ting, S.W. Chao, J. Mol. Catal. A: Chem. 235 (2005) 200–205.
[26] M. Xu, W. Wang, M. Seiler, A. Buchholz, M. Hunger, J. Phys. Chem. B 106 (2002) 3202–3208.
[27] Q. Xia, K. Hidajat, S. Kawi, J. Catal. 205 (2002) 318–331.
[28] J.M. Campelo, D. Luna, R. Luque, J.M. Marinas, A.A. Romero, J.J. Calvino, M.P. Rodríguez-Luque, J. Catal. 230 (2005) 327–338.
[29] R. Luque, J.M. Campelo, D. Luna, J.M. Marinas, A.A. Romero, Micropor. Mesopor. Mater. 84 (2005) 11–20.
[30] O.A. Anunziata, M.L. Martínez, M.B. Gómez Costa, Mater. Lett. 64 (2010) 545–548.
[31] D. Cunha, G. Cruz, Appl. Catal. A: Gen. 236 (2002) 55–66.
[32] G. McVicker, M. Daage, M. Touvelle, C. Hudson, D. Klein, W. Baird, B. Cook, J. Chen, S. Hantzer, D. Vaughan, E. Ellis, O. Feeley, J. Catal. 210 (2002) 137.
[33] M. Arribas, P. Concepcion, A. Martínez, Appl. Catal. A: Gen. 267 (2004) 111.
[34] U. Nylen, J.F. Delgado, S. Jaras, M. Boutonnet, Appl. Catal. A: Gen. 262 (2004) 189.
[35] R. Frety, P. da Silva, M. Guenin, Appl. Catal. 57 (1990) 99.
[36] M.J. Dees, A.J. den Hartog, V. Ponec, Appl. Catal. 72 (1991) 343.
[37] T.A. Pecoraro, R.R. Chianelli, J. Catal. 67 (1981) 430.
[38] S. Eijsbouts, V.H.J. de Beer, R. Prins, J. Catal. 109 (1988) 217.
[39] Z. VõÂt, M. ZdrazÏil, J. Catal. 119 (1989) 1.
[40] H. Topsoe, B.S. Clausen, F.E. Massoth, Catal. Sci. Technol. (1996) 11.
[41] K. Herbst, M.l. Brorson, A. Carlsson, J. Mol. Catal. A: Chem. 325 (2010) 1–7.
[42] R.C. Santana, P.T. Do, M. Santikunaporn, W.E. Alvarez, J.D. Taylor, E.L. Sughrue, D.E. Resasco, Fuel 85 (2006) 643.
[43] C.C.C. Augusto, J.L. Zotin, A.C. Faro Jr., Catal. Lett. 75 (2001) 37.
[44] Z. Vít, M. ZdrazÏil, J. Catal. 119 (1989) 1.
[45] J. Cinibulk, Z. VõÂ, Appl. Catal. A: Gen. 180 (1999) 15–23.
[46] A. Drahoradova, E. Hillerova, Z. Hrzan, M.R. icanek, Z. Vít, Chem. Prum. 43 (1993) 93.
[47] S.J. Liaw, A. Raje, R. Lin, B.V. Davis, in: M.L. Ocelli, R.R. Chianelli (Eds.), Hydrotreating Technology for Pollution Control Catalysts, Catalysis and Processes, M. Dekker, NY, 1996, pp. 197–209.
[48] T.G. Harvey, K.C. Pratt, Appl. Catal. 47 (1989) 335.
[49] K.C. Mouli, V. Sundaramurthy, A.K. Dalai, J. Mol. Catal. A: Chem. 304 (2009) 77–84.

[50] K. Foger, J.R. Anderson, J. Catal. 59 (1979) 325.
[51] V. Ponec, Adv. Catal. 32 (1983) 149.
[52] J. Barbier, P. Marecot, J. Catal. 102 (1986) 21.
[53] J. Barbier, P. Marecot, L. Tifouti, Appl. Catal. 19 (1985) 375.
[54] M.J. Girgis, B.C. Gates, Ind. Eng. Chem. Res. 30 (1991) 2021–2058 (and references therein).
[55] E. Furimsky, F.E. Massoth, Catal. Today 52 (1999) 381–495 (and references therein).
[56] F. Van Looij, P. Van der Laan, W.H.J. Stork, D.J. DiCamillo, J. Swain, Appl. Catal. A: Gen. 170 (1998) 1–12.
[57] G.C. Laredo, J.A. De los Reyes, J.L. Cano, J.J. Castillo, Appl. Catal. A: Gen. 207 (2001) 103–112.
[58] M. Nagai, T. Kabe, J. Catal. 81 (1983) 440–449.
[59] E.O. Odebunmi, D.F. Ollis, J. Catal. 80 (1983) 76–89.
[60] D. Dong, S. Jeong, F.E. Massoth, Catal. Today 37 (1997) 267–275.
[61] B. Muegge, F.E. Massoth, Fuel Process. Technol. 29 (1991) 19–30.
[62] S.H. Yang, C.N. Satterfield, Ind. Eng. Chem. Proc. Des. Dev. 23 (1984) 20–25.
[63] V. LaVopa, C.N. Satterfield, J. Catal. 110 (1988) 375–387.
[64] T.-W. Kim, R. Ryoo, M. Kruk, K. Gierszal, M. Jaroniec, S. Kamiya, O. Terasaki, J. Phys. Chem. B 108 (2004) 11480.
[65] D. Zhao, Q. Huo, J. Feng, B.F. Chmelka, G.D. Stucky, J. Am. Chem. Soc. 120 (1998) 6024.
[66] S. Wu, Y. Han, Y.C. Zou, J.W. Song, L. Zhao, Y. Di, S.Z. Liu, F.S. Xiao, Chem. Mater. 16 (2004) 486.
[67] J.C. Amezcua, L. Lizama, C. Salcedo, I. Puente, J.M. Domınguez, T. Klimova, Catal. Today 107–108 (2005) 578.
[68] J. Aburto, M. Ayala, I. Bustos-Jaimes, C. Montiel, E. Terres, J.M. Domınguez, E. Torres, Micropor. Mesopor. Mater. 83 (2005) 193.
[69] C.-F. Cheng, Y.-C. Lin, H.-H. Cheng, Y.-C. Chen, Chem. Phys. Lett. 382 (2003) 496.
[70] P. Van Der Voort, M. Benjelloun, E.F. Vansant, J. Phys. Chem. B 106 (2002) 9027.
[71] X.S. Zhao, G.Q. Lu, G.J. Millar, Ind. Eng. Chem. Res. 35 (1996) 2075.
[72] S. Laha, R. Kumar, Micropor. Mesopor. Mater. 53 (2002) 163.
[73] F. Chen, A. Shen, X.-J. Xu, R. Xu, F. Kooli, Micropor. Mesopor. Mater. 79 (2005) 85.
[74] A.V. Sapre, B.C. Gates, Ind. Eng. Chem. Res. 20 (1980) 68–73.
[75] S.C. Korre, M.T. Klein, R.J. Quann, Ind. Eng. Chem. Res. 34 (1995) 101–107.
[76] G. Laredo, J. De los Reyes, L. Cano, J. Castillo, Appl. Catal. A: Gen. 207 (2001) 103.
[77] J.L. Olive, S. Biyoko, C. Moulinas, P. Geneste, Appl. Catal. 19 (1985) 165.
[78] Z. Sarbak, React. Kinet. Catal. Lett. 32 (1986) 449.
[79] T.C. Ho, Catal. Rev. Sci. Eng. 30 (1988) 117.
[80] E.O. Odebunmi, D.F. Ollis, J. Catal. 80 (1983) 76.
[81] D. Dong, S. Jeong, F.E. Massoth, Catal. Today 37 (1997) 267.
[82] B. Muegge, F.E. Massoth, in: C.H. Bartholomew, J.B. Butt (Eds.), Catalyst Deactivation, Elsevier, Amsterdam, 1991, p. 297.
[83] S.H. Yang, C.N. Satterfield, Ind. Eng. Chem. Proc. Des. Dev. 23 (1984) 20.